

SANDIA REPORT

SAND2004-8153
Unlimited Release
Printed March 2004

Final-Part Metrology for LIGA Springs, Build Group 1

G. Aigeldinger, J. T. Ceremuga, B. E. Mills, D. M. Skala

Prepared by
Sandia National Laboratories
Albuquerque, New Mexico 87185 and Livermore, California 94550

Sandia is a multiprogram laboratory operated by Sandia Corporation,
a Lockheed Martin Company, for the United States Department of Energy's
National Nuclear Security Administration under Contract DE-AC04-94AL85000.

Approved for public release; further dissemination unlimited.



Sandia National Laboratories

Issued by Sandia National Laboratories, operated for the United States Department of Energy by Sandia Corporation.

NOTICE: This report was prepared as an account of work sponsored by an agency of the United States Government. Neither the United States Government, nor any agency thereof, nor any of their employees, nor any of their contractors, subcontractors, or their employees, make any warranty, express or implied, or assume any legal liability or responsibility for the accuracy, completeness, or usefulness of any information, apparatus, product, or process disclosed, or represent that its use would not infringe privately owned rights. Reference herein to any specific commercial product, process, or service by trade name, trademark, manufacturer, or otherwise, does not necessarily constitute or imply its endorsement, recommendation, or favoring by the United States Government, any agency thereof, or any of their contractors or subcontractors. The views and opinions expressed herein do not necessarily state or reflect those of the United States Government, any agency thereof, or any of their contractors.

Printed in the United States of America. This report has been reproduced directly from the best available copy.

Available to DOE and DOE contractors from
U.S. Department of Energy
Office of Scientific and Technical Information
P.O. Box 62
Oak Ridge, TN 37831

Telephone: (865)576-8401
Facsimile: (865)576-5728
E-Mail: reports@adonis.osti.gov
Online ordering: <http://www.doc.gov/bridge>

Available to the public from
U.S. Department of Commerce
National Technical Information Service
5285 Port Royal Rd
Springfield, VA 22161

Telephone: (800)553-6847
Facsimile: (703)605-6900
E-Mail: orders@ntis.fedworld.gov
Online order: <http://www.ntis.gov/help/ordermethods.asp?loc=7-4-0#online>



Final-Part Metrology for LIGA Springs, Build Group 1

Georg Aigeldinger and Joseph Ceremuga
Microsystems Processing Department

Bernice Mills
Analytical Materials Science Department

Dawn Skala
Advanced Lithography Department

Sandia National Laboratories
P. O. Box 969
Livermore, California 94550

Abstract

The LIGA spring is a recently designed part for defense program applications. The Sandia California LIGA team has produced an initial group build of these nickel alloy parts. These are distinctive in having a macroscopic lateral size of about 1 cm, while requiring microscopic dimensional precision on the order of a few micrometers. LIGA technology capabilities at Sandia are able to manufacture such precise structures. While certain aspects of the LIGA process and its production capabilities have been dimensionally characterized in the past, [1-6] the present work is exclusive in defining a set of methods and techniques to inspect and measure final LIGA nickel alloy parts in large prototype quantities. One hundred percent inspection, meaning that every single LIGA part produced needs to be measured, ensures quality control and customer satisfaction in this prototype production run.

After a general visual inspection of the parts and an x-ray check for voids, high precision dimensional metrology tools are employed. The acquired data is analyzed using both in house and commercially available software. Examples of measurements illustrating these new metrology capabilities are presented throughout the report. These examples furthermore emphasize that thorough inspection of every final part is not only essential to characterize but also improve the LIGA manufacturing process.

Acknowledgements

The authors would like to thank Nancy Yang, Sandia CA, for arranging for user time on a Jeol 6700 SEM and for supplying a custom mount for LIGA springs.

All x-ray lithography exposures for the fabrication of the first build of LIGA springs have been conducted at the Advanced Light Source, Berkeley, CA. The Advanced Light Source is supported by the Director, Office of Science, Office of Basic Energy Sciences, Materials Sciences Division, of the U.S. Department of Energy under Contract No. DE-AC03-76SF00098 at Lawrence Berkeley National Laboratory.

Table of Contents

INTRODUCTION.....	7
INSTRUMENTATION	9
INSPECTION OF UNRELEASED NICKEL ALLOY PARTS.....	11
OPTICAL MICROSCOPE VISUAL INSPECTION BEFORE RELEASE	11
X-RAY INSPECTION OF PARTS ON WAFER	12
INSPECTION OF RELEASED PARTS	14
QUALITATIVE OPTICAL INSPECTION	14
SIDEWALL ROUGHNESS AND TOPOLOGY – APPLIED TO ENTIRE WAFER BATCH	14
LATERAL DIMENSIONAL METROLOGY OF LIGA SPRINGS	18
COMPARISON OF CLOUD DATA WITH CAD.....	19
PART HEIGHT MEASUREMENT	21
TOP AND BOTTOM SURFACE TOPOLOGIES	22
DATA PACKAGE SUPPLIED TO THE CUSTOMER	25
CONCLUSIONS – OUTLOOK	27
REFERENCES.....	28

(This page intentionally left blank)

Final-Part Metrology for LIGA Springs

Build Group 1

Introduction

Deep x-ray lithography followed by electroforming is capable of producing high precision parts with high aspect ratio [7]. LIGA was invented in Germany and is the German acronym for lithography (Lithographie), electroforming (Galvanoformung) and molding (Abformung) [8]. The method of directly using the synchrotron mold for part production has generally been called “direct LIGA“ [9].

Figure 1 shows a photograph of a batch of springs produced by the LIGA technique.



Figure 1: Picture of a batch of springs produced by the LIGA technique. Final gold plated parts.

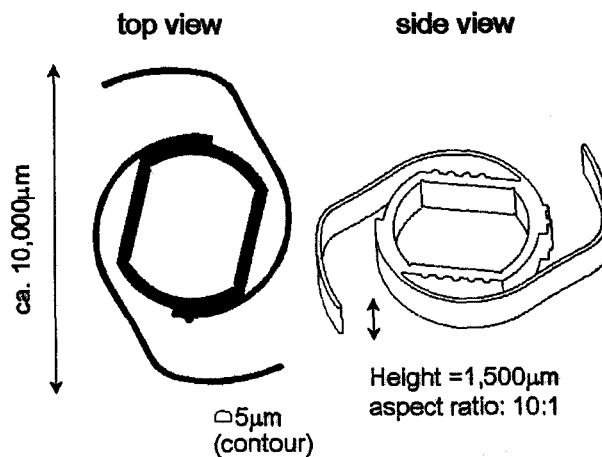


Figure 2: Drawing of the LIGA spring. Note the large overall size, the high aspect ratio and the small tolerances required.

These are nickel alloy electroformed parts, which have been gold coated by electroplating as a final process step. Obvious is the high aspect ratio of the spring arms, which are only $150\ \mu\text{m}$ wide but $1500\ \mu\text{m}$ tall. Lateral shapes can be designed freely using LIGA technology. This means that the spring's mechanical parameters and specifications can be designed to an optimum for its application. Figure 2 shows a drawing of a spring in top and side view. Note the large lateral dimensions and the overall $\pm 5\ \mu\text{m}$ contour tolerance called out by the customer.¹ Measuring the part with high precision over the area of about

¹ Definition of contour tolerance or profile tolerancing: “The condition where a tolerance zone is established by a three dimensional zone extending the length and width, or circumference of the considered feature”. [10]

1 cm² [11] is one of the main challenges in this work. There are more parameters of interest and many more inspection steps necessary.

Figure 3 shows a principal sketch of a typical LIGA part. Indicated are the dimensions of interest to achieve comprehensive metrology ensuring sufficient quality control and providing valuable feedback to processing for both control and improvement.

Figure 4 shows a flow diagram mapping the general route that every LIGA spring takes through the metrology process. This report will describe each one of these steps in detail. The instrumentation to facilitate these measurements and inspection steps are introduced in the following chapter.

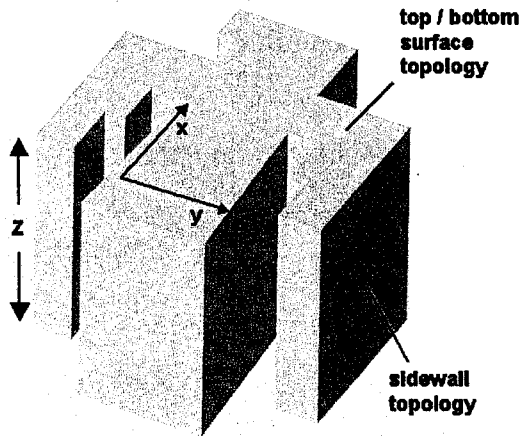


Figure 3: Principal sketch of a released nickel alloy LIGA part. Indicated are the dimensions and aspects of the part that are of interest for inspection.

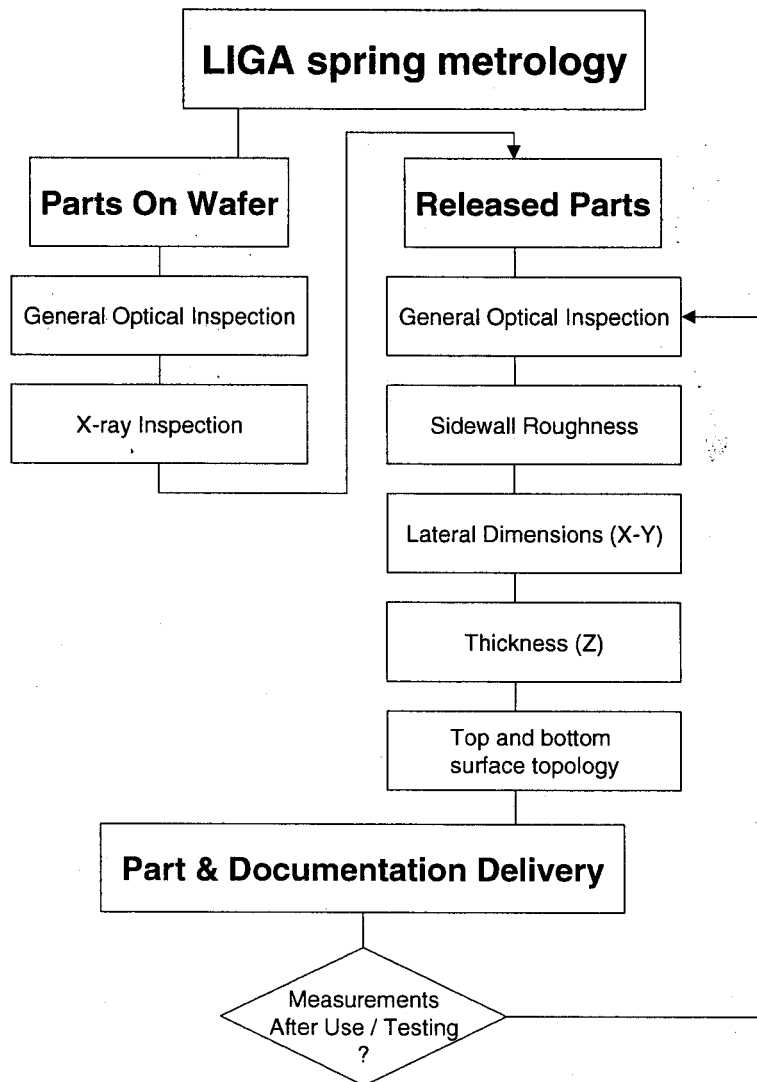


Figure 4: General flow of LIGA spring parts through the various inspection steps.

Instrumentation

In preparation for extensive metrology and process control, a set of tools for high precision LIGA part inspection and dimensional metrology were procured. For determining lateral dimensions on the top and bottom surface of the parts, an optical measuring-microscope was acquired: the View Engineering Voyager 6x12 system is fully programmable for repeat measurements and is suited for high throughput applications [12]. Figure 5 shows a picture of the instrument in the LIGA metrology laboratory. With an integrated video camera in the microscope optics, it allows for software edge detection and analysis of the measurement data. The high precision X-Y stage enables the use of high-resolution optics for the determination of edges in the sub micrometer range and for moving the large part to find other edges. This way, while the large lateral dimension of typical LIGA parts can be accommodated, the entire part can be inspected, keeping high resolution during edge finding. The microscope's software measures basic geometries like linewidths, radii and distances. It also gives the option of saving all captured data as point clouds, individual x, y, z coordinates

for each measured point. The point cloud data can be processed after the measurement is complete. Once the instrument has been programmed for a certain part, only two edges on the part have to be found manually. After this alignment step, the instrument will precisely align a part-coordinate system and measure in the pre-programmed locations in this coordinate system.

The manufacturer's specifications are $0.1\ \mu\text{m}$ lateral resolution (achieved through sub-pixelation algorithms) and a $3.5\ \mu\text{m}$ overall accuracy. For the LIGA spring a $20\times$ objective was chosen, giving a pixel size corresponding to approximately $0.5\ \mu\text{m}$. Using this objective on a chrome master, $150\ \mu\text{m}$ linewidths could be measured with repeatability better than $0.2\ \mu\text{m}$. The repeatability across the entire area ($6''\times 12''$) when stage movement is introduced is better than $0.5\ \mu\text{m}$.



Figure 5: View Engineering V6x12 Dimensional Microscopy System.

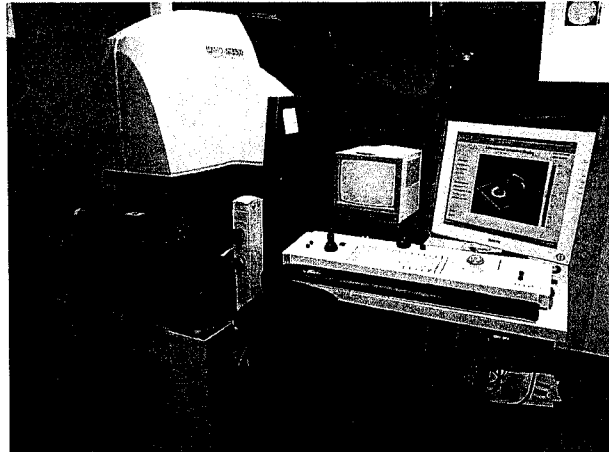


Figure 6: Wyko NT 3300 Interferometric Microscope

For determining the part surface topology, a Wyko white light interferometric microscope has been acquired [13]. A picture of the equipment can be seen in Figure 6. This instrument allows measurements of part surface roughness with a resolution of $0.1\ \text{nm}$. A recent upgrade with a high precision X-Y stage allows for the inspection of large LIGA part topologies on the order of $1\ \text{cm}^2$ in lateral size. While this instrument captures part topology on flat surfaces very well, the optics limit the angle of the part surface to about 10 degrees out of plane. The reference beam has to be reflected back into the microscope optics. This means that the instrument cannot inspect arbitrary surfaces, only steps, roughness and nominally flat topologies. This instrument also requires the specimen to be reflective; a condition LIGA fabricated nickel alloy parts easily meet.

Other instruments used for LIGA metrology are:

- Vision Industries Inspection microscope, variable objective from 6x-40x
- Nikon MM-40 with Metronics software (objective: 5,10,20 and 50x)
- Jeol 6700 scanning electron microscope with Jeol linewidth measurement software
- Tencor mechanical profilometer
- Heidenhain CP25M digital high precision indicator over base (thickness gauge)

Inspection of Unreleased Nickel Alloy Parts

Optical Microscope Visual Inspection before Release

After x-ray exposure at the synchrotron and development of the PMMA mold, a copper release layer, about 6-10 μm thick is electroplated into the bottom of the mold. Then the nickel alloy is electrodeposited into the mold. The parts are typically “over-plated” to ensure complete filling of the mold. The top surface of the wafer is ground and subsequently lapped and polished to the final part thickness, allowing for the release layer thickness. A mirror smooth surface with a roughness typically less than 500nm Ra is achieved as a final top surface by polishing.² After these steps are completed, and before the PMMA or the parts are released, the wafer is inspected.

While the springs are still on the wafer, typical top surface roughness is taken to assure a smooth finish. Then each spring is inspected under the Vision Engineering inspection microscope with a 40x objective setting. Any surface defects, e.g. from low plating spots are mapped in a wafer CAD layout map. This step is taken to trace potential problems to overall layout geometries.

² Ra is the average roughness as calculated over the entire measured array. Ra is calculated per the ANSI B46.1

standard:
$$R_a = \frac{1}{n} \sum_{i=1}^n |Z_i - \bar{Z}|$$

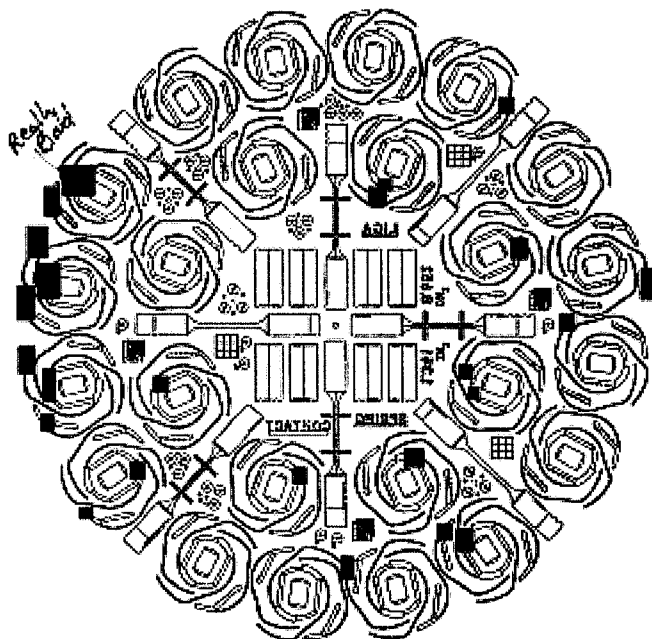


Figure 7: Example of a map used for basic inspection of an unreleased wafer. Problem zones are marked (black rectangles) and labeled where necessary.

Figure 7 shows an example of a map of one of the first LIGA spring wafers fabricated. Problem zones are marked, e.g., defective top surfaces from “under-plating”, which are areas where there was not enough nickel deposited to fill the mold to the top edge. Generally, areas with as little as 5 μm material missing from the top surface can be identified by this method. This basic inspection provides valuable wafer based data and feedback to the processors. For example, a probability of defects depending on location on the wafer can be easily revealed with this recording method.

X-ray Inspection of Parts on Wafer

After a basic optical inspection, the wafer is examined by radiography to check for voids in the electroplated material. Bubble-induced voids have generally been a problem in LIGA electrodeposits. They occur most likely in deep features when the feature aspect ratio is large. For such features, diffusive limitations on the rate of metal ion transport yield low current efficiencies and large hydrogen evolution when the current density is large [14]. Low current densities, however, also yield low efficiencies due to the increased kinetics of hydrolysis (relative to metal deposition) at low over-potentials. As such, there may exist only a small range of current densities for which bubble formation is unlikely. These optimum conditions are sometimes difficult to discern, leading to some parts being produced with voids.

Parts are generally inspected on-wafer after they have been lapped and polished. The wafer is placed in contact with double 5”x7” films (single side coated film available from Kodak). Defects in the part must be seen in both films to be considered. One image is taken with the wafer plane normal to the 0.5 mm focal spot x-ray beam, at a source to film distance of 1.37 m. The Faxitron x-ray source is operated at 80 kV and at a fluence of approximately 30 mA•min (10 min at 3mA) [15]. The precise fluence required depends on the exact

parameters of the sample, e.g. the wafer material. For a contact print, the distance from the x-ray source to the top of the part is nearly 1000 times the distance from the top of the part to the film, thus the maximum projection error due to beam divergence is about 0.1%.

Two more images are taken with the wafer plane at 25° to the x-ray beam: One at a 0°, the other at a 90° rotation of the wafer. These films are exposed at 60 kV and 45mA•min. This angled exposure is taken at lower energy because the beam passes through less areal density of nickel alloy. This angled exposure results in a "side view" radiograph that allows better visualization of flaws in the highest aspect ratio portion of a part (i.e. the spring arms). The exposed and developed films are inspected with the aid of 7x or 10x comparators. To document flaw free parts, the normal angle exposure films are scanned on a drum scanner at 3000dpi. A print of the x-ray image, enlarged to standard page size, is delivered with every spring's data package.

Small numbers of released parts can also be inspected in the same manner as entire wafers, by supporting the parts with a plastic straightedge. Larger numbers of released parts can be temporarily adhered to a wafer or they can be inspected loosely in the horizontal plane on the film. In this case, instead of tilting the film and wafer for the angled exposure, the x-ray beam is tilted and the parts are staged on a 6 µm Mylar film that is stretched tight in a 12" diameter hoop.

A map like the one in Figure 7 is prepared to indicate any voids or other flaws that may occur. A list is also prepared with a description of the nature and position of each flaw; e.g., whether it is on the top or bottom surface with respect to the plating direction. Figure 8 shows an optical microscope picture of a spring next to the radiograph of the same spring. Although the spring shows only a small pit on the surface in the optical picture, that of the x-ray inspection reveals a very large internal void. Obviously, this spring will not pass inspection. While physical cross section and x-ray tomography results both indicate that bubbles generally leave defects of a minimum size that is easily detectable by x-ray inspection, work is under way to determine the flaw size that can be detected in the arms and bodies of the spring.

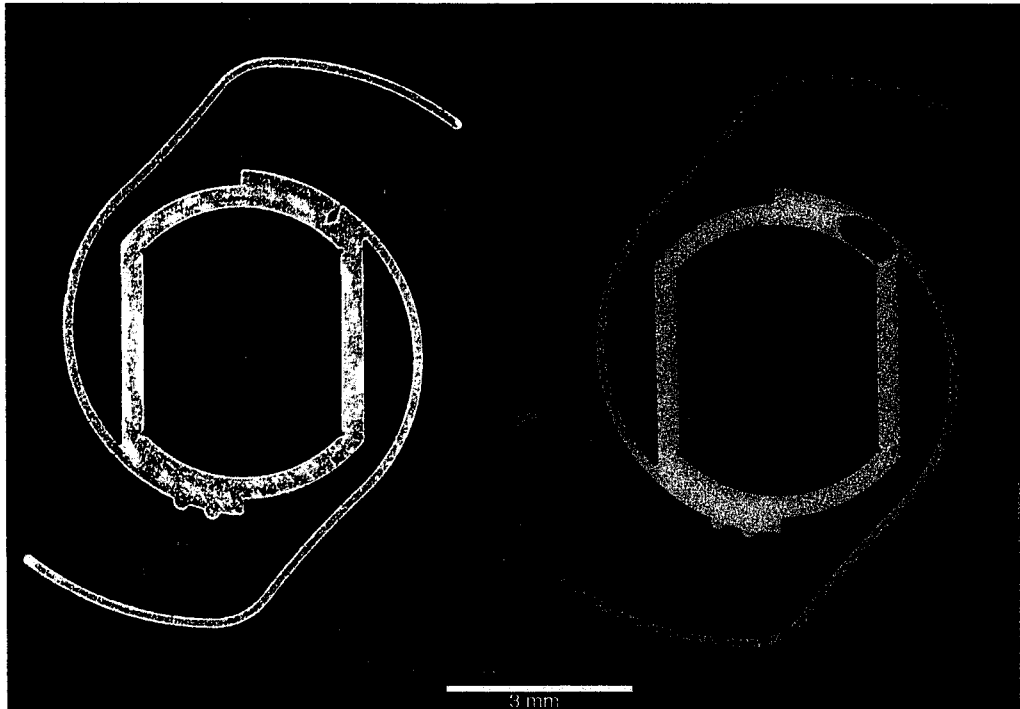


Figure 8: Comparison of optical and x-ray image of a spring. While a small void is visible in the optical inspection, x-rays reveal a very large internal void beneath it.

Inspection of Released Parts

Qualitative Optical Inspection

This inspection step ensures that any defects or imperfections that are not visible by other means are discovered. Examples of such imperfections may be large convex or concave striations on the sidewall stemming from a mask defect or burrs and bevels. This qualitative inspection method is also applied to the final gold plated part to ensure even gold coating with no pinholes or other defects. The inspection is conducted with the Vision Systems inspection microscope. The part is manipulated manually using self-locking carbon fiber tip tweezers and all visible surfaces are inspected.

Sidewall Roughness and Topology – Applied to Entire Wafer Batch

Sidewall roughness is an important parameter. X-ray lithography is capable of transferring nanometer scale features on a sidewall from the gold x-ray mask to the PMMA resist [1, 3]. While this attribute of x-ray lithography is used to produce high precision parts, it will also transfer any imperfections in the Au absorber sidewall to the PMMA resist. The electroplated nickel alloy also replicates these nanometer scale features. Although increased sidewall

roughness in the nickel parts is generally generated in the x-ray lithography step, by copying mask imperfections, there are some other factors determining surface roughness. For example micro-cracks in the PMMA resist would also be replicated in the parts [16].

Sidewall roughness inspection is performed with the Wyko interferometer. For this purpose, a preferably straight sidewall that is easily accessible is chosen. Figure 9 shows a typical measurement of a sidewall on a flat part of a LIGA spring wafer. The data is visualized in a shade-coded map with the shade going from white (highest points) to black (lowest points).

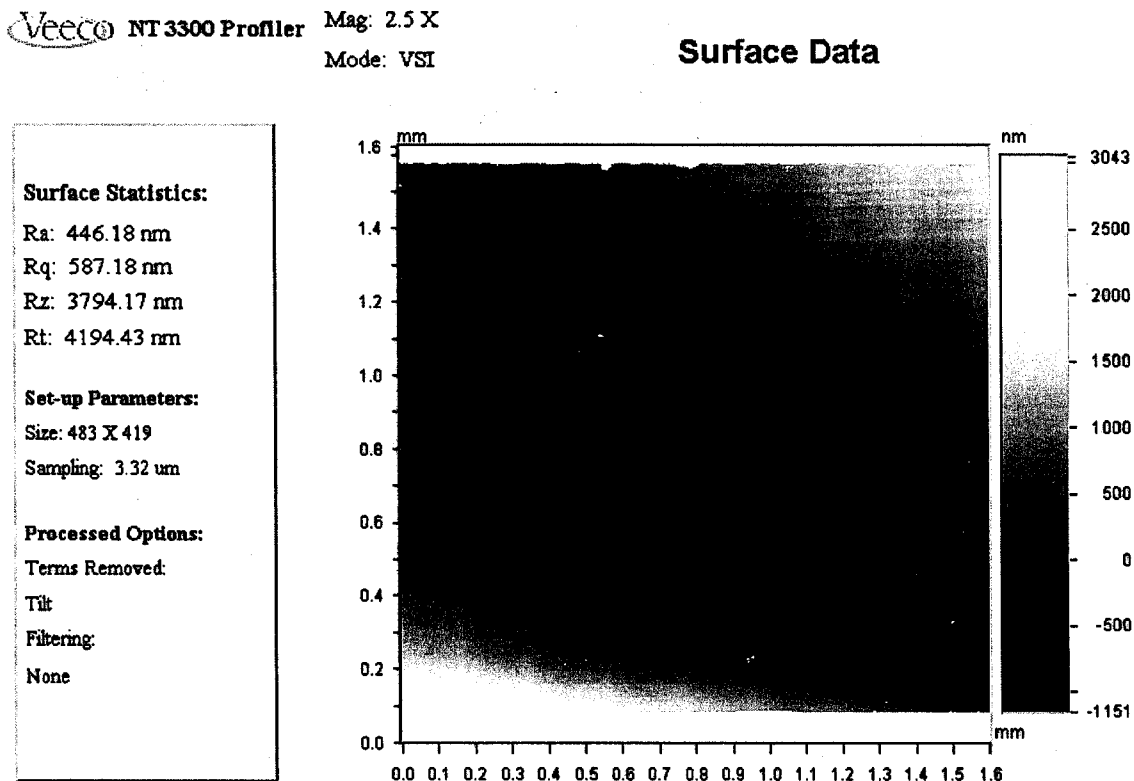


Figure 9: Sidewall surface scan of a sample part off a LIGA spring wafer measured with the Wyko NT3300. The area sampled is 1.6 mm x 1.6 mm while the amplitude of surface variation from black to white is approximately 4 μm . The vertical striations that are visible are on the order of 200 nm. The top of the structure (lapped side) is up, bottom (released side) is down.

The average roughness of such a large area is typically 500 nm Ra or better. Note that a true roughness measurement is made on a smaller scale, where topology does not skew the measurement. In Figure 9 note the overall twist of the nominally flat sidewall of ca. 4 μm . This deformation is likely caused by stress in the deposit. The stress of the deposit is not higher in a tall structure, but the large overall dimension of the structure leads to a larger absolute displacement [17].

There are arbitrarily frequent vertical striations that must have been transferred to the PMMA resist in the x-ray lithography step, because they run exactly parallel to the direction of the x-rays. The repetitive vertical striation pattern that appears about every 200 μm is possibly transferred from the chrome master, which is e beam written. In the beam writing process,

polygons or trapezoids are combined to form the actual pattern. There is also generally a stitching error of the electron beam writer, which can lead to dose variations in the stitching locations. Both traits of the e beam writing process can lead to edge effects where the trapezoids or beam writer fields meet [18]. The amplitude of these surface imperfections is on the order of 200 nm and of no concern for this application. If more precisely written and more costly chrome on glass masters were used, these effects could possibly be reduced. This effect will need to be examined in more detail in the near future.

There is some horizontal grain visible that is likely introduced during electroplating. It is not well understood why electrodeposition of the structure can lead to such a variation in sidewall topology. This effect is small, being less than 100 nm in amplitude, but should be investigated more closely.

It must be noted that these horizontal striations are not a replication of sidewall cracks in the PMMA resist. Sidewall cracking in PMMA typically is not present on the entire structure and does not run completely parallel to the plating direction, rather than fan out into other directions [16]. PMMA cracks also would replicate with more amplitude and steeper grades in the nickel deposit sidewall. Typically, PMMA cracks can be seen with the Wyko interferometer if present. Processing has been optimized to avoid cracks in PMMA on the order of microns or several hundred nm, which could compromise the functionality of the spring.

The measured sidewall roughness in the sample part is recorded and given as an overall value for the wafer. New designs of masks now include “dummy” components where key features of parts are designed and produced for the sole purpose of good sidewall measurement access. Figure 10 shows the vertical sidewall profile extracted from center of the structure dataset in Figure 9. The lapped side of the part is on the bottom, the polished side on the top.

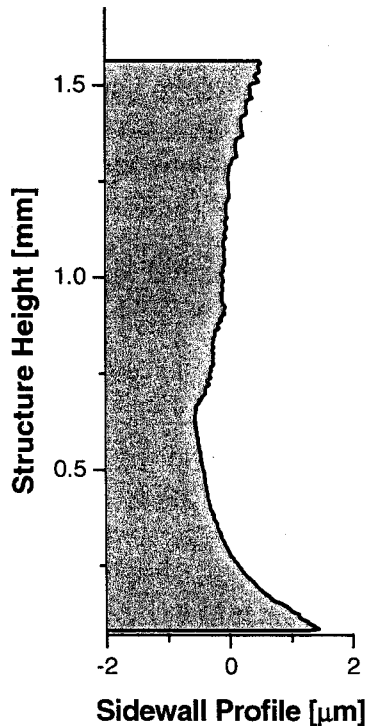


Figure 10: Sidewall Profile Measured with the Wyko NT3300 profilometer. Note that this profile may be superimposed on an actual slope, since the tilt is automatically removed and there is no reference to the top and bottom planes of the structure.

This concave (ca. $2\mu\text{m}$ over the $1500\mu\text{m}$ structure height) sidewall profile with a larger footing on the bottom, is typical, resulting partly from the ultra-deep x-ray lithography process. While the primary dose in the PMMA resist is uniform, which would result in a practically straight sidewall profile, there are secondary radiation effects leading to increased dose on the bottom of the PMMA, which reflects in more material in the electroplated structures [2, 19-21]. Also, during electrodeposition, the PMMA resist tends to swell, affecting the top of the mold most because it is exposed to the electrolyte the longest and is not directly attached to the substrate. This swelling generally results in narrowing of the electroplated part towards the top [6, 22-24].

It is very important to note that the profile shown does not necessarily lie on a plane normal to the substrate surface or bottom surface of the structure as the dataset shown may indicate. The instrument software removes the general tilt of all examined data. This means that the profile can be superimposed to a general slope that is not visible in the shown profile.

One way to capture the true shape of the sidewall, including slope, is to measure top and bottom width of the part on the view microscope and then combine the data with the sidewall profile. Preliminary tests reveal that the sidewall width measurements on the View microscope are not accurate enough (currently estimated to be less than 2 microns using coaxial light, due to edge detection in a 3 dimensional part) to reach any conclusive results.

Another possibility for capturing the true sidewall slope and shape is to use cuboid LIGA structures and place them on their side on a flat carrier. Then the entire geometry is scanned,

from the bottom flat, through the sidewall facing up. This will produce a dataset showing the actual combined sidewall slope of the structure. Preliminary studies show that slight warpage of parts from internal stress (like shown in Figure 10) will not allow the part to lay flat on its sidewall, making accurate measurements in the micron and sub micron range impossible.

The problem of measuring sidewall slope, especially with respect to top and bottom surfaces of the part needs to be addressed. Currently one relies on the fact that during x-ray exposure, the mask and wafer are aligned within a few milliradians normal to the incoming x-ray beam, so that there is no general skew present from a slanted exposure. It would be desirable to verify this in the metrology of the final part.

Lateral Dimensional Metrology of LIGA springs

After release, single springs are inspected using the View Voyager optical microscope. The top (lapped and polished) and bottom (released) surfaces of the springs are examined. The microscope is capable of performing direct metrology of basic geometries and saving edge detection data of entire parts. In the direct measurement of geometries, simple shapes like arcs, circles, linewidths, and lengths can be captured. For the LIGA spring, body widths, arc diameters and arm widths are measured in this fashion. Since the part is used as a spring, arm linewidths are a crucial dimension to inspect. The width is checked across the nominally 150 μ m wide arm. Typical direct measurements are indicated in Figure 11. The instrument saves the dimensions extracted from measured points in an ASCII text file.

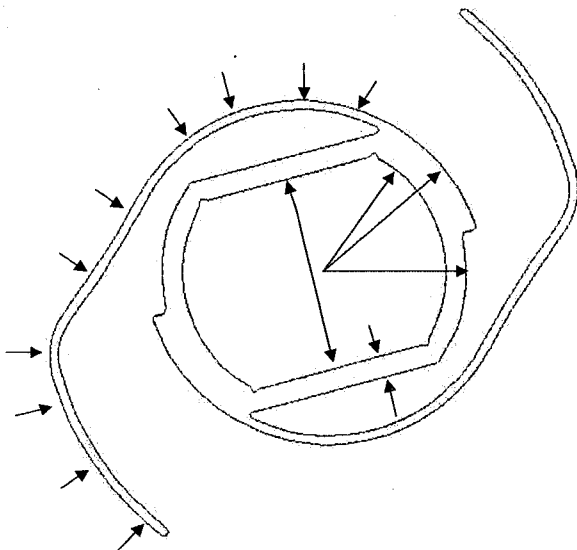


Figure 11: Directly measured geometries include 10 arm widths per arm, inner and outer hub radii, and widths on the inner body of the spring.

Both Figure 12 and Figure 13 show arm width measurements taken from a set of springs generated from a single wafer. The x-axis represents the number of the data set. The data set consists of the average and standard deviation ($\pm\sigma$) of all twenty armwidth measurements taken from both arms, from the arm root to the arm tip.

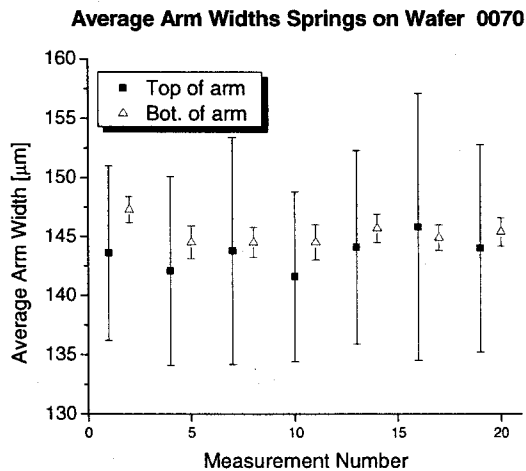


Figure 12: Average arm widths of springs from wafer 0070. The average top values are considerably smaller than the bottom while having very large standard deviations.

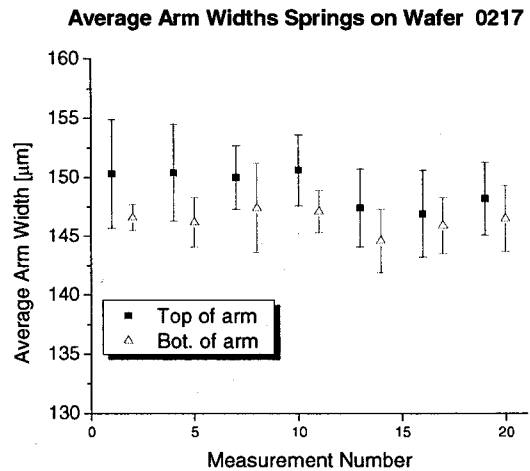


Figure 13: Average arm widths of springs from wafer 0217. Note the improvements vs. wafer 0070: average widths are now closer to nominal and standard deviations are lower on the top surface measurements. This was achieved by introducing auxiliary structures neighboring the spring arms.

In Figure 12, measurements for a wafer produced early in the process are shown. It is visible that the top arm widths are less than the bottom widths of the arm. This results from the swelling effects of the surrounding PMMA during electroplating [6, 22-24]. Thus, the top of the structures becomes narrower than the bottom. In addition, the large standard deviation indicates that this effect is not uniform along the length of the arm. This can be explained by the fact that the roots and tips of the arm are not affected as much from PMMA swelling as the center areas of the arm. Figure 13 shows the same measurements taken for a wafer fabricated later in time. It has an improved design implemented in the layout: auxiliary structures are introduced to form trenches around the part in PMMA. The mass of the PMMA that swells is reduced and narrowing of the arm width is reduced [6, 23, 24]. The average value and the standard deviation of the top measurements are now much closer to the desired 150 μm.

While auxiliary features can greatly decrease swelling effects, narrowing top widths of structures, there are limitations. In the example of the spring, auxiliary structures could only be placed to the outside of the arms and not to the inside. The area to the inside of the arm is physically blocked by the hub of the spring. The hub's geometry is not an ideal auxiliary feature and unwanted swelling effects remain.

Comparison of Cloud Data with CAD

The instrument saves all points found during the measurement procedure. The point clouds taken during the LIGA spring metrology consist of over 4000 points per part surface. Figure 14 shows a plot of the coordinate point cloud. Measurement locations were positioned

strategically to sufficiently complete inspection requirements. If desired, entire wafers (of unreleased parts or molds) can be captured, resulting in clouds of over 100,000 points. Figure 15 shows an example of a point cloud where an entire wafer was inspected (unreleased parts).

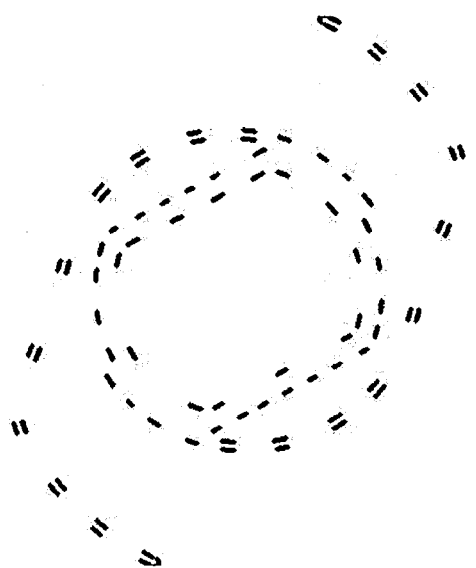


Figure 14: Point cloud of a spring. Each cluster represents an edge measurement location, consisting of many points. This results in a cloud of over 4000 points total.

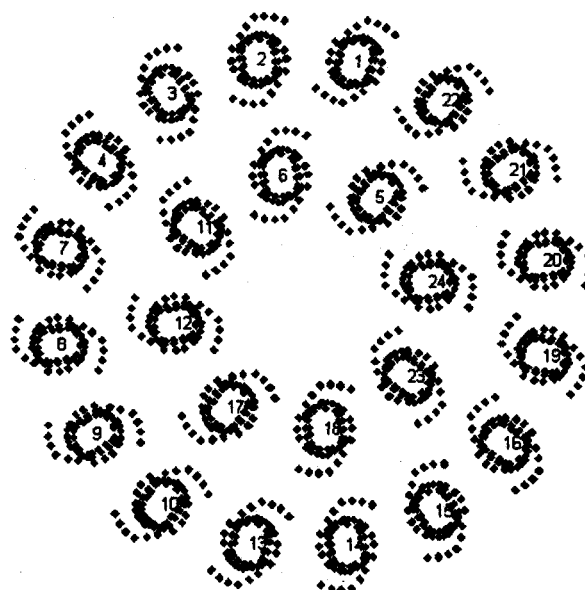


Figure 15: A point cloud representing an entire wafer of unreleased spring parts. There are over 100,000 points plotted in this picture.

This point cloud data is then mathematically fit to the computer aided design (CAD) model to ensure the entire contour of the part conforms to design specifications. This data analysis step is performed using a commercially available software package [25]. The software allows the linear least squares fit of point clouds to part geometry. In the case of the LIGA spring, the center hub geometry is weighted in the fitting algorithm to properly align the data to the CAD model. The deviations of the point cloud data with respect to the CAD model is visualized by drawing the CAD model and connecting the points to the model with vectors called “whiskers” or “spikes”. These are lines drawn from the points normal to the corresponding boundary on the CAD.

Figure 16 shows an example of a whisker plot. The errors seen are exaggerated by a factor of twenty. On whiskers plots, the software allows deviations to be visualized in different colors, depending on whether they are into the part solid or away from the part solid.

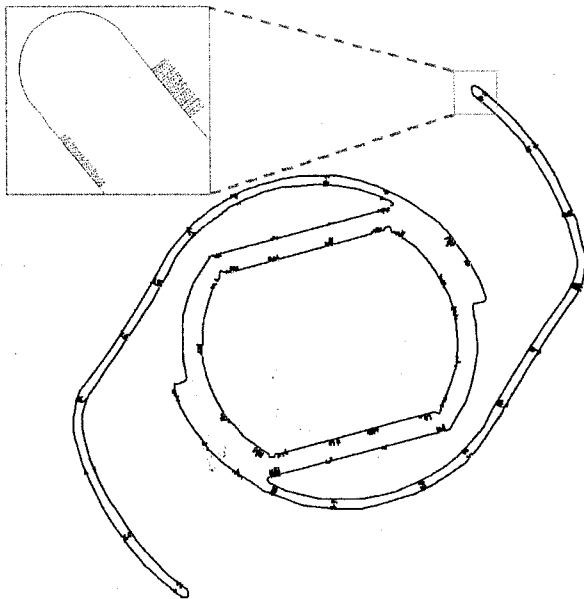


Figure 16: CAD (solid line) to point comparison. The points measured are connected to the model with normal lines. The lines are normal to the CAD model. The lines are 20 times exaggerated to make very small errors visible.

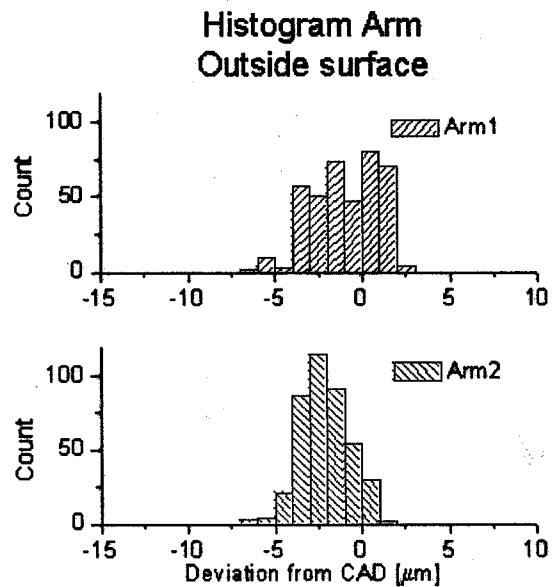


Figure 17: Histogram of outside arm surface deviations from CAD.

Once the overlay of the point cloud to the CAD model is performed and displayed, the deviations are exported and summarized in a histogram. Again, certain key geometries of the part can be chosen for analysis. Figure 17 shows the histograms for outer surface points on the spring arms. It is clearly visible that the deviations are within the desired $\pm 5\mu\text{m}$ contour tolerance.

Part Height Measurement

The overall Z height of these rather large parts is sampled in four locations using a digital high precision indicator over base gauge (Heidenhain CP25M). Spring parts are large and rugged enough to be manipulated with tweezers when taking care to only handle the body of the springs and not the arms. The arms are not sampled because they may be deformed in the process. If the arms would be lower than the spring's hub, this would be indicated in the topology measurements, which are discussed in the next chapter.

Figure 18 shows the 4 sampling points used for the thickness measurements. Generally, the springs are sampled on top and bottom. The measurements are combined to a total thickness reported with the standard deviation of the data. Figure 19 shows an example of 13 springs measured off one wafer.

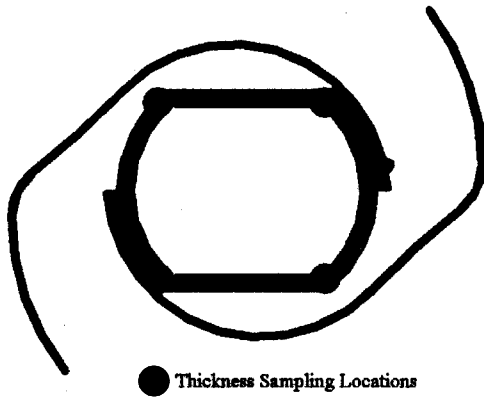


Figure 18: Locations on spring on which thickness sampling is performed.

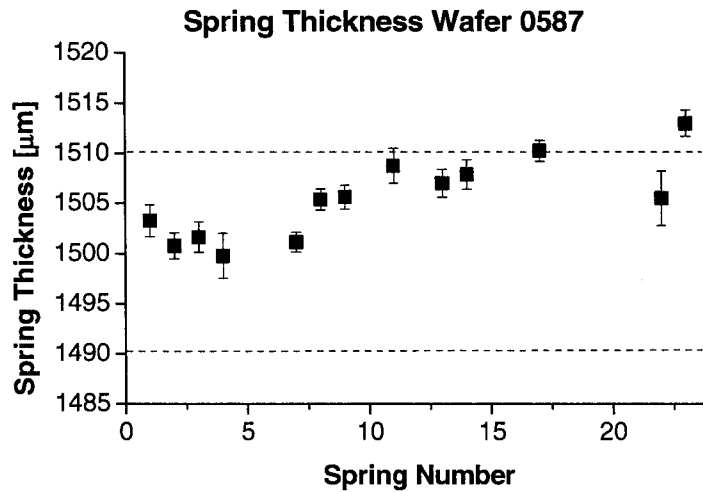


Figure 19: Thickness of 13 Springs off one wafer. The errors are standard deviations of the 8 points measured. The dashed lines indicate the part's thickness specification.

Top and Bottom Surface Topologies

With the Wyko NT3300, top and bottom topologies of the parts can be captured in one measurement by using the XY stage movement and stitching software. This measurement ensures flatness of the part before delivery. Figure 20 shows a spring fabricated in an early mold. The arms of the spring are about 25 µm lower, than the center hub section of the spring. This undesirable topology results from the fact that thin arms are having soft PMMA surrounding them during lapping with no other support and being lapped more than the thicker parts on the spring. This is reduced by a factor of five by adding auxiliary features around the spring arms, which support the arms during lapping. A much-improved topology of a later spring (where auxiliary features were present during lapping) is shown in Figure 21.

Surface Data

Surface Statistics:
 Ra: 3221.06 nm
 Rq: 4899.71 nm
 Rz: 25780.53 nm
 Rt: 27805.30 nm

Set-up Parameters:
 Size: 743 X 570
 Sampling: 13.30 um

Processed Options:
 Terms Removed:
 Tilt
 Filtering:
 None

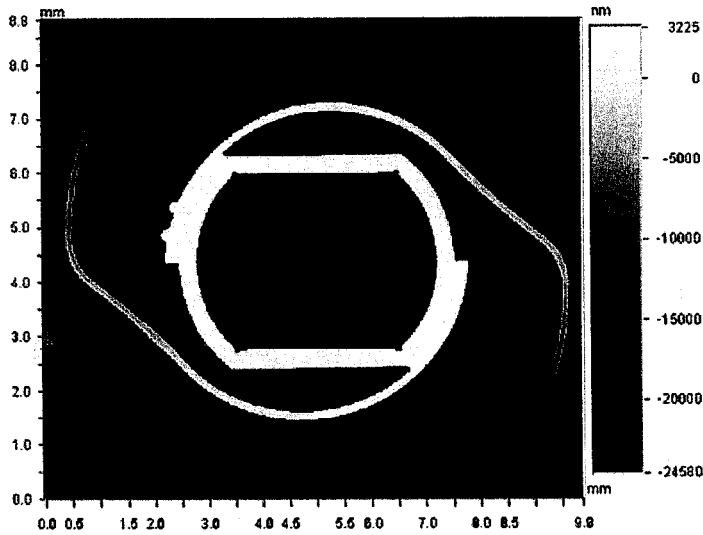


Figure 20:
 Surface topography of the lapped side of a spring measured with the Wyko NT3300. The arms of the springs are approximately 25 μm lower than the center body.

Surface Data

Surface Statistics:
 Ra: 637.50 nm
 Rq: 769.04 nm
 Rz: 4488.33 nm
 Rt: 5050.64 nm

Set-up Parameters:
 Size: 1472 X 977
 Sampling: 6.77 um

Processed Options:
 Terms Removed:
 Tilt
 Filtering:
 None

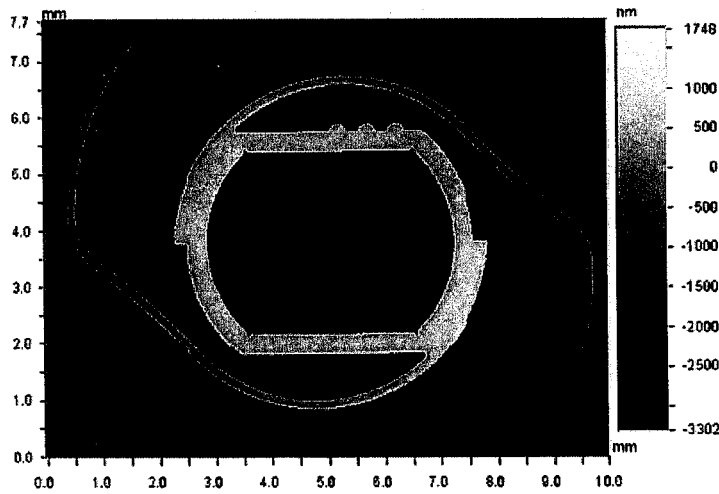


Figure 21:
 Surface topography of the lapped side of a spring measured with the Wyko NT3300. The arms of this spring are only 5 μm lower than the center body due to the auxiliary structures that are supporting the arms during lapping.

If there are surface imperfections visible in the qualitative optical inspection, the interferometer is also used to quantify them. Figure 22 shows surface imperfections on a bottom (released side) of a spring. The left shows an SEM image compared to the interferometric image to the right. The interferometer reveals that the circular shaped imperfections are high spots of approximately 9 μm in height.

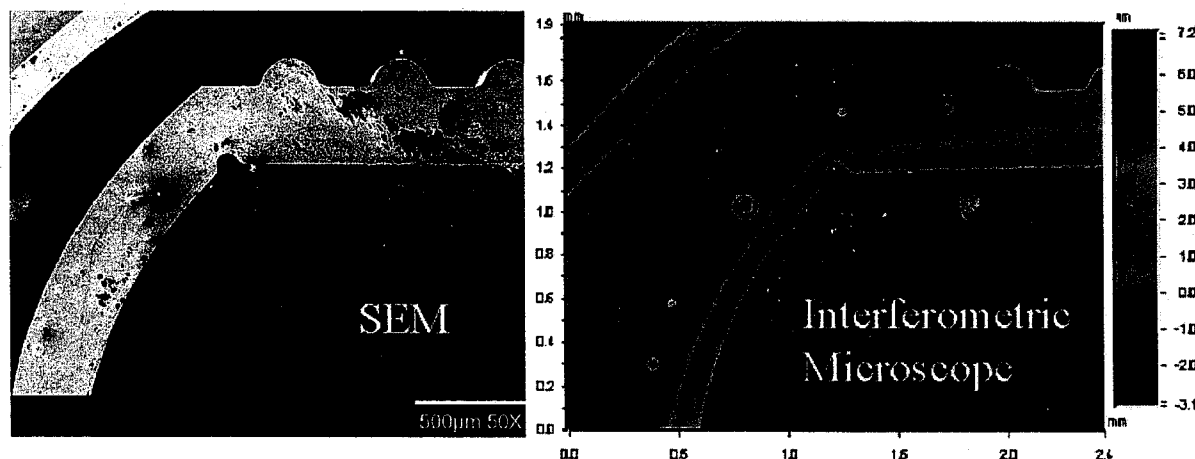


Figure 22: Comparison of SEM image (left) to interferometric image (right) taken with the Wyko tool. In this example bottom side (released side) imperfections are being quantified using the interferometric microscope. The thermal scale on the topology plot ranges from -3 to 7 μm . Imperfections shown is high spots (circular) of about 9 μm .

A bubble in the copper release layer likely creates these effects. The copper release layer is electroplated first, into the bottom of the mold. If this layer has a bubble, no copper will be present in a circular area. Once transferred to the nickel bath, the bubble likely bursts and nickel plates into the void. This will lead to a plateau like structure with a circular pattern, having the height of the copper strike layer. 9 μm is a common thickness for the copper release layer in manufacturing these springs.

Data Package Supplied to the Customer

For each wafer, a parts disposition log accounts for each part and these are the reports the customer is supplied with for each spring at time of delivery:

- **Wafer:**
 - Aerial map of the optical inspection for voids and imperfections (top surface).
 - Interferometric images of the sidewall quality and average roughness for the wafer.
 - Summary sheets for various data.
- **Every Part:**
 - An inspection log sheet as a cover accompanies the extensive data package collected for each spring. The log sheet summarizes all captured data in one view. A sample is shown in Figure 23 to illustrate the detail of inspection going into every part delivered to customer.
 - Plotted top and bottom surface topologies of the spring.
 - Possible imperfections on any surface are also recorded using the interferometer.
 - Thickness data.
 - Dimensional analysis data for top and bottom arm widths of spring.
 - Contour overlay with CAD for top and bottom of spring.
 - Contour histogram plots for both top and bottom measurements. The histograms are separated into four different plots: inside hub, arm 1, arm 2 and all data.

Overall, the metrology report for each spring consists of about 10 pages of data, while the wafer information adds about 10 pages to the report. Such extensive metrology data is useful to quantify the LIGA process and performance as the process becomes more mature. In the long term, it is unlikely that such extensive metrology will be needed, or even desired, due to cost considerations.

Inspection Log

Wafer # _____ Part _____ Part # _____ Material NiMn

Optical Inspection
 Visual Presence Only
 Operator _____
 Date _____
 Magnification _____
 Top _____
 Bottom _____

Dimensional Analysis

1. Top & Bottom

Operator _____
 Date _____
 Magnification _____
 System _____

	Top	Bottom
Slot width	_____	_____
Inner Radius	_____	_____
Arm width range	_____	_____

2. Part Thickness

Operator _____
 Date _____
 System / Method _____

3. Surface Finish

Operator _____
 Date _____
 System _____
 Magnification _____
 Top Ra _____
 Bottom Ra _____
 Sidewall Ra (typical for wafer) _____

Au coated: Visual Inspection for Voids
 Operator _____
 Magnification _____
 Date _____

Comments:

Accept _____ Accept (Conditional) _____ Reject _____

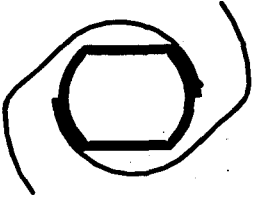


Figure 23: Sample log sheet supplied with data package to customer.

Conclusions – Outlook

An innovative part inspection capability and procedure has been successfully established for the metrology of LIGA springs. The procedure includes many instruments and methods in order to capture all acquirable aspects of the challenging geometry. In addition to ensuring that well-characterized quality parts are delivered to the customer, it could be shown through examples how valuable metrology can be by helping to understand the effect of process materials and conditions on part morphology.

Future work will determine the uncertainty of the metrology instruments beyond manufacturer's specifications. Standards and calibration will need to be emphasized also, since currently only yearly manufacturer's calibrations are in place, with basic in-house checks added to the calibration schedule.

Streamlining data analysis and data reduction will be addressed. This is especially important when moving the part from a prototype to a production part.

With respect to general LIGA research, the established metrology capabilities will be of great help to quantify and qualify more process parameters. For example, PMMA resist swelling will be examined more closely and sidewall roughness effects will be studied in detail using the LIGA spring as a vehicle.

References

1. Mohr, J., W. Ehrfeld, and D. Munchmeier, *Requirements on Resist Layers in Deep-etch Synchrotron Radiation Lithography*. Journal of Vacuum Science and Technology B, 1988. **6**(6): p. 2264-2267.
2. Feiertag, G., et al., *Calculation and experimental determination of the structure transfer accuracy in deep x-ray lithography*. Journal of Micromechanics and Microengineering, 1997. **7**(4): p. 323-331.
3. Achenbach, S., J. Mohr, and F.J. Pantenburg, *Application of Scanning Probe Microscopy for the determination of the structural accuracy of high aspect ratio microstructures*. Microelectronic Engineering, 2000. **53**: p. 637-640.
4. Dearth, B.L. and R.G. Steinhoff, *LiGA measurement and acceptance evaluation*. Microsystem Technologies, 2003. **9**(3): p. 197-203.
5. Aigeldinger, G., et al., *Studying Stacked Ultra Deep X-ray Lithography Exposures: Preliminary Results*. Proceedings of the Society of Photo-Optical Instrumentation Engineers (SPIE), 2001. **4557**: p. 85-92.
6. Aigeldinger, G., J. Ceremuga, and D. Skala, *Large Batch Dimensional Metrology Demonstrated in the Example of a LiGA Fabricated Spring*. Book of Abstracts, HARMST 2003, USA, 2003: p. 263-264.
7. Hruby, J., *LiGA Technologies and Applications*. MRS Bulletin, 2001. **26**(4): p. 337-340.
8. Becker, E.W., et al., *Fabrication of microstructures with high aspect ratios and great structural heights by synchrotron radiation lithography, galvanofforming, and plastic moulding (LiGA process)*. Microelectronic Engineering, 1986. **4**: p. 35-53.
9. Guckel, H., et al., *Direct high throughput LiGA for commercial applications: a progress report*. Microsystem Technologies, 2000. **6**(3): p. 103 - 105.
10. Puncochar, D.E., *Interpretation of Geometric Dimensioning and Tolerancing*. 2nd ed. 1997, New York, New York: Industrial Press Inc.
11. Dewa, A.S., *Mesosopic systems: bridging from micromachined devices to macroscopic systems*. Mechatronics, 1998. **8**(5): p. 521-534.
12. *View Engineering. Company Homepage: <http://www.vieweng.com>, Visited 02/04.*
13. *Veeco / Wyco. Company Homepage: <http://www.veeco.com>, Visited 02/04.*
14. Griffiths, S.K., et al., *Transport Limitations in Electrodeposition for LiGA Microdevice Fabrication*. Proceedings of the Society of Photo-Optical Instrumentation Engineers (SPIE), 1998. **3511**: p. 364-375.
15. *Faxitron Company Homepage: <http://www.faxitron.com>, Visited 02/04.*
16. Pantenburg, F.J., S. Achenbach, and J. Mohr, *Characterisation of defects in very high deep-etch X-ray lithography microstructures*. Microsystem Technologies, 1998. **4**(2): p. 89-93.
17. Safranek, W.H., *The Properties of Electrodeposited Metals and Alloys*. 2nd ed. 1986, Orlando, FL: American Electroplaters and Surface Finishers Society.
18. McCord, M.A. and M.J. Rooks, *Handbook of Microlithography, Micromachining and Microfabrication*. Electron Beam Lithography, ed. P. Rai-Choudhury. Vol. 1. 1997: SPIE Optical Engineering Press. 142-249.

19. Pantenburg, F.J. and J. Mohr, *Influence of secondary effects on the structure quality in deep X-ray lithography*. Nuclear Instruments and Methods in Physics Research, Section B, 1995. **97**(1-4): p. 551-556.
20. Griffiths, S.K. and A. Ting, *The influence of X-ray fluorescence on LIGA sidewall tolerances*. Microsystem Technologies, 2002. **8**. (2-3): p. 120-128.
21. Pantenburg, F.J. and S.K. Griffiths, *Measurement of LIGA Resist Line Width Deviations*. Book of Abstracts, HARMST 2003, USA, 2003: p. 67-68.
22. Goods, S.H., R.M. Watson, and M. Yi, *Thermal Expansion and Hydration Behaviour of PMMA Molding Materials for LIGA Applications I*. SAND REPORT, Sandia National Laboratories, 2003(2003-8000).
23. Ruzzu, A. and B. Matthis, *Swelling of PMMA-structures in aqueous solutions and room temperature Ni-electroforming*. Microsystem Technologies, 2002. **8**(2-3): p. 116 - 119.
24. Griffiths, S.K. and J.A.W. Crowell, *Dimensional Errors in LIGA-Produced Metal Parts due to Thermal Expansion and Swelling of PMMA*. Book of Abstracts, HARMST 2003, USA, 2003: p. 93-94.
25. ICAMP Company web site: <http://www.icamp.com>, visited 02/04.

Distribution:

- 3 Center for Advanced Microstructures and Devices
Attn: J. Goettert
Y. Desta
V. Singh
6980 Jefferson Highway
Baton Rouge, LA 70803

- 1 Georgia Institute of Technology
Attn: T. R. Kurfess
MARC 435
813 Ferst Drive N.W.
Atlanta, GA 30332

- 4 Honeywell Federal Manufacturing & Technologies
Attn: Robert G. Steinhoff
Sherri Huffman
Madhuri Widmar
D. L. Dearth
PO Box 419159
Kansas City, MO 64141

- 1 IMTEK-Institut für Mikrosystemtechnik
Attn: W. Menz
Georges-Köhler-Allee 103
79110 Freiburg
GERMANY

- 4 Institut für Mikrostrukturtechnik
Attn: V. Saile
J. Mohr
F. J. Pantenburg
P. Meyer
Forschungszentrum Karlsruhe
Hermann-von-Helmholtz-Platz 1
76344 Eggenstein-Leopoldshafen
GERMANY

- 1 Osservatorio Astronomico di Brera
Attn: M. Ghigo
Via E. Bianchi 46,
23807 Merate (LC)
ITALY

1 National Synchrotron Light Source
Attn: E. Johnson
P. O. Box 5000, Bldg. 725D
Upton, New York 11973

1 U.S. Department of Energy
Attn: Craig C. Henderson
NA-115/Forrestal Building
1000 Independence Avenue, SW
Washington, DC 20585

1 MS0196 R. Wild, 2618
1 MS0319 J. R. Fellerhoff, 2610
1 MS0319 D. E. Petersen, 2618
1 MS0319 C. W. Vanecsek, 2618
1 MS0437 C.L. Knapp, 2120
1 MS0437 J. M. McGlaun, 2830
1 MS0503 D.W. Plummer 2330
1 MS0561 T. T. Smith 14111
1 MS0889 S. V. Prasad, 1851
1 MS0958 G. L. Benavides 14184
1 MS1007 J. Jones, 15272
1 MS1007 L. Shippers, 15272
1 MS1310 S. N. Kempka, 9113
1 MS1310 M. A. Polosky, 2614

1 MS9001 M. E. John, 8000; Attn:
MS9004 R. H. Stulen, 8100
MS9007 D. R. Henson, 8200
MS9054 W. J. McLean, 8300
MS9002 P. N. Smith, 8500
MS9003 K. E. Washington, 8900

1 MS9005 B. K. Damkroger, 8240
1 MS9036 M. A. Forman, 8245
1 MS9161 W. R. Even, 8760
1 MS9403 J. M. Hruby, 8700
1 MS9404 G. D. Kubiak, 8750
1 MS9401 J. E. M. Goldsmith, 8751
1 MS9401 M. A. Hekmaty, 8751
1 MS9401 L. L. Hunter, 8751
1 MS9401 K. D. Krenz, 8751
1 MS9401 M. E. Malinowski, 8751
1 MS9401 S. Mrowka, 8751
5 MS9401 D. M. Skala, 8751
1 MS9401 A. A. Talin, 8751

20	MS9401	G. Aigeldinger, 8753
1	MS9401	D. R. Boehme, 8753
1	MS9401	G. F. Cardinale, 8753
5	MS9401	J. T. Ceremuga, 8753
1	MS9401	J. T. Hachman, 8753
1	MS9401	J. J. Kelly, 8753
1	MS9401	D. E. McLean, 8753
1	MS9401	T. I. Wallow, 8753
1	MS9401	P. C. Y. Yang, 8753
1	MS9042	G. H. Evans, 8752
1	MS9042	S. K. Griffiths, 8752
1	MS9042	R. S. Larson, 8752
1	MS9042	C. D. Moen, 8752
1	MS9042	R. H. Nilson, 8752
1	MS9042	A. Ting, 8752
1	MS9403	L. A. Domeier, 8762
5	MS9403	B. E. Mills, 8773
1	MS9403	A. M. Morales, 8762
1	MS9403	N. Y. C. Yang, 8773
1	MS9405	K. L. Wilson, 8770
1	MS9409	J. R. Garcia, 8754
1	MS9409	S. H. Goods, 8754
1	MS9409	J. S. Korellis, 8754
1	MS9409	W.Y. Lu, 8754
3	MS9018	Central Technical Files, 8945-1
1	MS0899	Technical Library, 9616
1	MS9021	Classification Office, 8511, for Technical Library, MS0899, 9616 DOE/OSTI via URL